# Performance of Different Water-Based Binder Formulations for Ni-Rich Cathodes Evaluated in $LiNi_{0.8}Mn_{0.1}Co_{0.1}O_2$//Graphite Pouch Cells

*Ritu Sahore [a,#], Marissa Wood [a,1,#], Alexander Kukay [b], Zhijia Du [a], Kelsey M. Livingston [a], David L. Wood III [a], Jianlin Li [a,*]*

*[a]Oak Ridge National Laboratory, Electrification and Energy Infrastructures Division, Oak Ridge, Tennessee 37831, United States*

*[b]Bredesen Center for Interdisciplinary Research and Graduate Education, University of Tennessee, Knoxville, TN 37996, USA*

[*] **Corresponding author:** *Jianlin Li* (lij4@ornl.gov)

[#] These authors contributed equally.

[1] **Present address:** Lawrence Livermore National Laboratory, 7000 East Ave, Livermore, CA, 94550 USA

**Keywords:** Lithium-ion battery, Ni-rich NMC, Aqueous electrode processing, Pouch cells, Water-based binders

This manuscript has been authored by UT-Battelle, LLC, under contract DE-AC05-00OR22725 with the US Department of Energy (DOE). The US government retains and the publisher, by accepting the article for publication, acknowledges that the US government retains a nonexclusive, paid-up, irrevocable, worldwide license to publish or reproduce the published form of this manuscript, or allow others to do so, for US government purposes. DOE will provide public access to these results of federally sponsored research in accordance with the DOE Public Access Plan (http://energy.gov/downloads/doe-public-access-plan).

## Abstract

Water-based processing for lithium-ion battery electrodes is attractive due to its lower manufacturing cost and smaller environmental impact. However, multiple challenges associated with aqueous cathode processing have hindered commercial adoption. Polymeric binders are an important component of the electrode, and thus the choice of binders can alter electrode cycling performance significantly. In this work, four different water-based binder combinations are investigated for Ni-rich $LiNi_{0.8}Mn_{0.1}Co_{0.1}O_2$ (NMC811)-based cathodes, with a focus on the long-term electrochemical performance in practical-format full pouch cells. No additional pH-modulating additives were added to the aqueous cathode slurries, and no protective coatings were present on the cathode or aluminum current collector. Results are compared with the standard PVDF/NMP-based binder/solvent combination, used as a baseline. The influence of water-based binder type on slurry rheology and electrode microstructure are also discussed. All cells made by water-processing had worse rate performance compared to the baseline. However, the cell discharge capacity after 1000 U.S. Advanced Battery Consortium (USABC) cycles at C/3 charge/discharge rate was comparable to the baseline for two of the water-based cathode formulations (CMC & JSR, and LiPAA), demonstrating the potential viability of aqueous-processed Ni-rich cathodes at a commercial scale.

## Introduction

Polymeric binders constitute an important component of lithium-ion battery electrodes. Although they are described as an 'inactive' component of the electrode, the choice of binder can significantly affect the electrode's microstructure, electronic and ionic conductivity, and mechanical properties (flexibility, adhesion, and cohesion), which in turn affect electrochemical cycling performance.[1, 2] A binder must possess several characteristics for it to be employed in a battery electrode, including chemical and electrochemical stability at both ambient and elevated temperatures, high solubility in the slurry solvent, low cost, good rheological properties to prevent sedimentation and particle agglomeration, and the ability to impart good mechanical properties to the final coating.[3]

Polyvinylidene fluoride (PVDF) binder dissolved in N-methyl-pyrrolidone (NMP) solvent is typically used as the binder/solvent system in conventional lithium-ion cathode processing and can fulfil most of these characteristics. However, both components are expensive, and the need to recover evaporated NMP during the drying step further adds to the processing and capital cost.[4, 5] It has been reported that 421 kWh of electricity is required to evaporate and recover NMP for a 10 kWh pack.[6] Replacing NMP with water can enable ~25% reduction in energy consumption during electrode manufacturing, corresponding to a savings of 105 kWh in electricity.[5] In addition, depending on how this electricity is produced, significant amounts of carbon dioxide can be generated. For example, the carbon dioxide emissions from coal in 2019 was 2.21 pounds per kWh of electricity. Therefore, switching from NMP to aqueous processing corresponds to a reduction of 10,500 tons of carbon dioxide emission per year for a 1 GWh battery plant.[7] These advantages

make aqueous processing of electrodes a very attractive alternative.[8] However, the use of water in cathode slurry processing introduces several additional challenges, such as leaching of $Li^+$ ions from the cathode particles, which raises the pH of the slurry enough to cause corrosion of the aluminum current collector immediately upon contact.[9-11] This leads to poor adhesion of the cathode coating to the current collector, deposition of corrosion products on the cathode particles, and cracking of the coatings during drying due to hydrogen gas evolution from corrosion, all of which combined contribute to mechanical, electrical, and electrochemical degradation.[12, 13] As a result, the studies of new aqueous polymer binder systems are complicated by this leaching/corrosion issue, which prevents evaluation of the effects of their intrinsic properties on the mechanical and electrochemical properties of the resulting cathode coatings in isolation. Several mitigation strategies have been demonstrated to suppress these high pH and/or corrosion effects, such as adding small amounts (< 2 wt. %) of acids or acidic additives, coating the surface of the cathode particles, and coating the current collector with carbon.[14-19] While the use of these mitigation strategies is inevitable for relatively thick cathodes (>2 mAh $cm^{-2}$) to make the coatings reasonably handleable, for thinner coatings calendering can help eliminate corrosion-related coating defects.

In this work, we compare three water-based binder formulations for aqueous-processed $LiNi_{0.8}Mn_{0.1}Co_{0.1}O_2$ (NMC811) cathodes in terms of their impact on long-term electrochemical cycling performance in full pouch cells with standard graphite anodes, both at room temperature and 45 °C. To minimize the cathode coating parameters and allow the study to focus solely on the binder formulation, no pH modulating additives or protective coatings for the cathode or current collector were used. Calendering was employed to eliminate corrosion-related coating defects. Results are compared with a standard PVDF/NMP coating of similar loading. Rheology characterization of the resulting slurries and microstructure characterization of the dry composite cathodes are also presented.

## Experimental Details

*Electrode Preparation and Characterization*

Table 1 shows the detailed electrode composition of the cathodes made with three different water-based binders, as well as one baseline cathode made with PVDF (Solvay 5130) as the binder and NMP (Sigma Aldrich) as the solvent. NMC811 (Targray), carbon black (Denka Li-100), and the binder under investigation were combined and mixed to form homogenous slurries in a planetary mixer (Ross, PMD – ½). The three water-based binder formulations studied are: 1) Carboxymethyl cellulose or CMC (Acros Organics, M.W. 250,000, D.S. 0.9) and water-based PVDF Latex (Solvay, XD # 859, 25.2 wt. % solids) in a 1:4 weight ratio, where CMC is primarily a slurry thickener and the emulsion binder is for binding, 2) CMC (Acros Organics, M.W. 250, 000, D.S. 0.9) and a fluorine acrylic hybrid latex binder (TRD 202A, JSR Micro, 41 wt. % solids) in a 1:4 weight ratio, and 3) Lithiated polyacrylic acid (LiPAA, M.W. 450,000). All chemicals were used as received, except LiPAA which was prepared in-house. The LiPAA was made using a 6 wt. %

PAA solution in DI water (139.2400 g) and a 4 M LiOH solution (45.598 g) to obtain a 7.22 wt. % solution of LiPAA. Additional solvent (NMP or water) was added as needed during slurry preparation to achieve the appropriate viscosity. The obtained slurries were coated and dried using a pilot-scale slot-die coater (Frontier) to achieve an NMC811 areal loading between ~9.8 – 10.3 mg/cm$^2$. For the aqueous-processed cathodes, the Al foils were corona treated (Enercon Compak 2000) at 4.4 J/cm$^2$ before coating to improve slurry wetting.[20] All electrodes were calendered to ~35% porosity. Additional drying of all coatings (overnight at 115 °C for NMP-based, 140 °C for water-based) was performed to get rid of any residual moisture prior to cell assembly. All coatings produced were flexible enough to be wound into rolls, even without the calendering step. Matching graphite anode coatings (N:P ratio between 1.1 and 1.2, or 6.0 – 6.9 mg/cm$^2$) with a composition of 92 wt. % graphite (Superior Graphite 1520-T), 2 wt. % C-NERGY Super C65 (Imerys), and 6 wt. % PVDF (9300, Kureha) were prepared using a similar process.

Electrode microstructure was characterized using scanning electron microscopy (Zeiss Merlin) to determine the distribution of the conductive additive and binder within the cathode as a function of binder type.

To measure the adhesion strength of the coatings on the aluminum current collector, 180$^o$ peel tests were performed using a Mecmesin Friction Peel Tear Tester. For the tests, 1" wide electrode strips were fixed on a steel plate using double-sided 3M VHB tape. The samples were then peeled off at 10 mm/min. However, adhesion strength measurements could not be made due to the poor cohesion of these coatings. Instead of getting a clean peel of the coatings from the current collector, all coatings broke apart from within during the test, leaving half of the coating on the tape and half on the current collector. SEM images of the aluminum substrate after the peel test are shown in Figure S1.

Table 1. Summary of composition and loading of the cathode coatings investigated in this study.

| Coating ID | Solvent | NMC811 (wt. %) | Carbon black (wt. %) | Binder 1 (wt. %) | Binder 2 (Emulsion -type) (wt. %) | Slurry solids loading (wt.%) | Measured pH of slurry | Active material loading (mg/cm$^2$) |
|---|---|---|---|---|---|---|---|---|
| Baseline - PVDF | NMP | 90 | 5 | 5 | N.A. | 42.0 | N.A. | 10.0 |
| Aqueous – CMC & Latex | Water | 90 | 5 | 1 | 4 | 69.3 | 12.05 | 10.3 |
| Aqueous – CMC & JSR | Water | 90 | 5 | 1 | 4 | 57.9 | 11.97 | 9.8 |
| Aqueous - LiPAA | Water | 90 | 5 | 5 | N.A. | 48.6 | 11.88 | 10.2 |

*Cell assembly and electrochemical testing*

Single-layer pouch cells (~100 mAh) were assembled in a dry room with a relative humidity of ~0.1 %. Celgard 2325 was used as the separator, and 1.2 M $LiPF_6$ in 3:7 wt.% ethylene carbonate/ethyl methyl carbonate was used as the electrolyte. The amount of electrolyte added to each cell was calculated using a fill factor of 2 (i.e., twice the total pore volume of cell components (cathode, anode, and separator).[21] A total of six pouch cells were assembled for each cathode type

(three for rate-performance testing and three for cycle-life testing). The geometric areas of the cathode and anode were 47.2 and 50.1 $cm^2$, respectively.

Cells were placed under a stack pressure of 5 psi during cycling. To aid electrolyte wetting, pouch cells were first charged at C/10 for 15 min and then allowed to rest for 6 h before cycling. All cells were cycled between 2.5 V and 4.2 V using a constant current – constant voltage protocol (charged to 4.2 V using a constant current, then held at 4.2 V until the current dropped to C/20 before discharging) where 1C was 195 mA/g of NMC811. Three formation cycles were performed for each cell (C/10 charge, C/10 discharge) before rate performance or cycle life testing. Rate performance was evaluated by charging at C/5 and discharging at different rates between C/10 and 10C (5 cycles at each rate). Long-term cycle life testing was performed by charging and discharging at C/3 for 1000 cycles. All tests were conducted in an environmental chamber (Espec) at 30 °C using a Maccor battery cycler (Series 4000).

*Hybrid Pulse Power Characterization (HPPC) tests*

Pouch cells assembled for long-term cycle life evaluation were subjected to HPPC tests before cycling as well as after every 200 cycles to evaluate their dynamic power capability over their voltage range. Each cell was first charged to its upper cutoff voltage (4.2 V) at C/3. It was then discharged at C/3 for 18 mins, with a 1 h rest afterwards to allow the cell to reach equilibrium, followed by 10-second-long discharge (at 2C) and charge (at 1.5C) pulses. This C/3 discharge and 2C discharge/1.5C charge pulse application was then repeated 9 times (or until the cell reached the lower cutoff voltage limit of 2.5 V, which is why sometimes there are less than 9 data points). If the application of a charge/discharge pulse at a certain state-of-charge (SOC) reached the set upper/lower cutoff voltage limit, 4.2/2.5 V, those data points were discarded. Area specific impedance (ASI, $\Omega$-$cm^2$) at a certain SOC was then calculated by taking a ratio of the voltage drop during the discharge pulse at 2C and multiplying it by the geometric area of the electrode. The SOC was estimated from the open circuit voltage at the end of the 1 h rest step following the 18 min long C/3 discharge.

*Rheology of cathode slurries*

Small scale dispersion samples were mixed in a high-shear mixer (Netzsch Premier Technologies Model 50) by adding each component in parts and mixing for 10 mins at 1500 rpm. Each component was added and mixed separately to avoid agglomeration and ensure a homogenous dispersion was formed. Each dispersion was altered to be 48.6 wt. % solids to ensure comparability among samples. Once a homogenous sample was obtained, 20 mL of each dispersion was transferred to a rheometer (TA Instruments Discovery HR-3) fitted with a concentric cylinder geometry (bob and cup). Each sample was first conditioned at 5 $s^{-1}$ for 1 minute. This sample conditioning was followed by a 30 second rest before linear viscoelastic regime (LVR) and flow ramp tests were performed. LVR tests were performed because additional low shear viscosity behavior and information on the binder network within the slurry can be extrapolated from LVR tests. Amplitude sweeps were performed by holding the angular frequency constant at 100 rad $s^{-1}$ and varying the oscillation strain from 0.01% to 10%. Frequency sweep tests were performed by holding the oscillation strain at the calculated critical strain value while sweeping the angular

frequency from 100 rad $s^{-1}$ to 0.1 rad $s^{-1}$. Critical strain was calculated by correlating 95% of the maximum storage modulus value with the corresponding oscillation strain. Samples were rebuilt between amplitude and frequency sweeps by applying a constant angular frequency of 100 rad $s^{-1}$ and the calculated critical strain for a total of 15 minutes. Rebuilding the slurry between tests minimized potential hysteresis effects. Flow ramp tests were carried out by varying the shear rate from 0.1 $s^{-1}$ to 3000 $s^{-1}$. The shear response was then measured as a function of shear rate. The sample was again rebuilt before flow ramp tests were performed.

*Slurry pH*

To collect sample pH, dispersions were centrifuged at 4000 rpm (VWR) in 5 min increments until separation occurred, and the resulting filtrate was transferred to a vial. A porous glass pH probe (Fisher Scientific) was used to collect the sample pH.

## Results and Discussion

*Rheology of cathode slurries*

The viscoelastic behavior of the dispersions in both high-shear viscosity (HSV) and low-shear viscosity (LSV) regimes are both important factors during the coating and drying process. High-shear viscosity (>100 $s^{-1}$) can be used to determine dispersion behavior during the coating process where coating consistency and reproducibility are paramount. Low-shear viscosity (<1 $s^{-1}$) is important in determining the binding network present in the slurry. The storage modulus describes the elasticity of the material and therefore the energy that can be stored before plastic deformation occurs through degradation of the polymer bridges between particles in the slurry. Practically, LSV can also be correlated to the quality of the electrode edge contour and waste potential, as electrodes with a well-defined edge will require less material to be cut off, reducing the scrap rate.[16, 22-24]

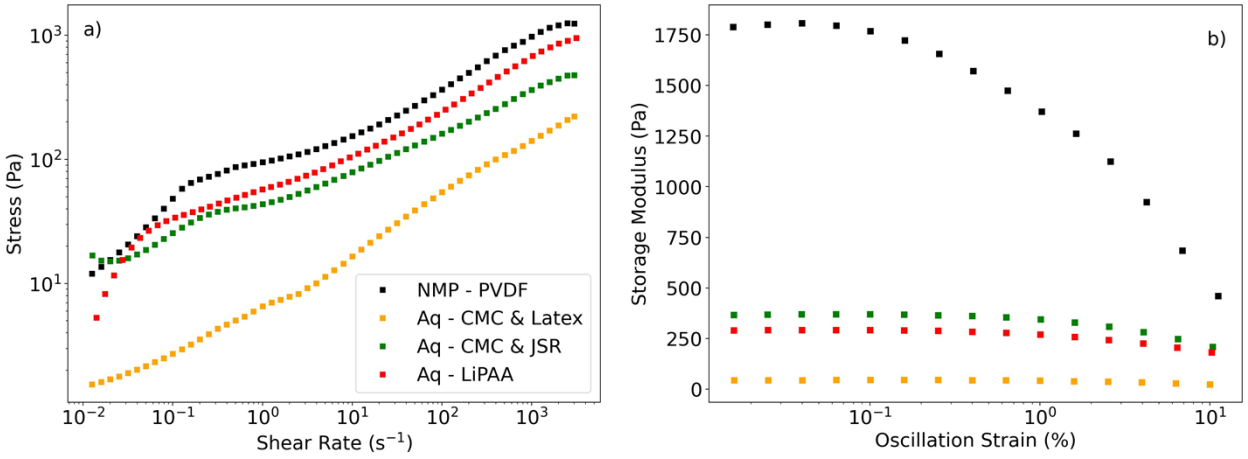


Figure 1. Stress as a function of shear rate collected from flow ramp tests and used to apply the Herschel-Bulkley model (a). Storage modulus as a function of oscillation strain (%) collected from linear viscoelastic regime tests

and used to describe the elastic component of slurry behavior at low shear rates (b). Slurry compositions used in these tests are listed in Table1.

As all samples exhibit shear-thinning behavior and can be described as generalized Newtonian fluids, the Herschel-Bulkley (H-B) model was applied to each composition (Figure 1a).[25] This model is in Equation [1], where $\tau$, $\tau_0$, K, $\dot{\gamma}$, and n represent the shear stress, yield stress, consistency index, shear rate, and power law index, respectively. In this model, the yield stress describes the stress required to initiate flow, and the extent of shear thinning is described by the power law index. For values of n less than 1, a sample is considered to be shear thinning. At n = 1, the equation reduces to the classical Bingham plastic equation. If n = 1 and $\tau_0 = 0$, the dispersion is considered Newtonian.[25] All samples exhibit a similar power-law index, ranging from 0.34 to 0.42, meaning each sample exhibits a similar degree of shear thinning behavior (Table 2). Notably, the CMC & Latex sample exhibited the highest power-law index and the lowest yield stress and consistency index. The yield stress reading of 0.00 Pa suggests this sample can be described by the power-law relation as well as the HB model. As the power-law index values are similar, the consistency indices of each sample can be compared to each other.[26] Since consistency index is related to the viscosity of the fluid, a comparison of viscosity can be made from these values. They show that the NMP-based sample is the most viscous, while the CMC & Latex sample is substantially less viscous than the other samples. This trend can also be observed in Figure 1a. This indicates that the solids loading in the aqueous slurries can be further increased without exceeding the viscosity of the NMP-based slurry. This would enable lower energy consumption and manufacturing cost.

$$\tau = \tau_0 + K\dot{\gamma}^n \quad \text{if } \tau > \tau_0 \qquad [1]$$

$$\dot{\gamma} = 0 \quad \text{if } \tau \leq \tau_0$$

Table 2: Herschel-Bulkley (H-B) model parameters for the four types of slurries.

| Coating ID | Solvent | Slurry Solids Loading (wt. %) | Power Law Index | Yield Stress (Pa) | Consistency Index | Calculated Critical Strain (%) |
|---|---|---|---|---|---|---|
| Baseline - PVDF | NMP | 48.6 | 0.37 | 8.16 | 70.17 | 0.01 |
| Aqueous - CMC & Latex | Water | 48.6 | 0.42 | 0.00 | 7.52 | 0.1 |
| Aqueous - CMC & JSR | Water | 48.6 | 0.34 | 9.78 | 32.19 | 0.1 |
| Aqueous - LiPAA | Water | 48.6 | 0.40 | 11.28 | 38.91 | 0.1 |

*Linear Viscoelastic Regime*

The sample with the lowest storage modulus was the CMC & Latex-based composition, suggesting the edge formation of the resulting electrode may be less defined and may lead to a less robust binding network (Figure 1b).[27] Conversely, the baseline NMP/PVDF composition exhibited a considerably higher storage modulus compared to all aqueous dispersions, which suggests that PVDF provides superior low-shear benefits that result in a more established binding network and higher stability in the slurry. This increased binding network should be more resistant to the plastic

deformation experienced in high shear rate applications, as the polymer to particle binding sites should be more robust.

*Microstructure characterization*

The surfaces of the uncalendered coatings were imaged with SEM (Figure 2) to understand the impact of binder type on the coating microstructure and electrochemical performance. Images at three different magnifications are shown for all four types of coatings. The distribution of carbon black and binder across the coating thickness was similar to the distribution on the surface (Figure S2). As expected, cracks and pinhole-type defects were observed on the surface of the aqueous-processed coatings, which have been shown to be caused by hydrogen gas evolution due to corrosion of the aluminum substrate by the highly basic (pH > 11) water-based slurries.[12] However, the baseline coating processed with NMP solvent shows no surface defects. Interestingly, the LiPAA aqueous-processed coating also did not show any surface defects despite the high pH of the corresponding slurry. This slurry did not have a particularly high solids loading (Table 1), which could have led to crack-free drying due to the lower water content in such a scenario as shown by Ibing et. al.[28] One possible explanation is the nature of the distribution of carbon black and binder within the coating. The carbon black and binder network in the LiPAA coating is distributed *in between* the NMC811 particles similar to that of the PVDF/NMP coating, which allows for more efficient utilization of this network to bind the particles compared to the CMC & Latex and CMC & JSR coatings, where the carbon black/binder network has completely engulfed the particles. The coverage of NMC811 particles is significantly greater in the case of CMC & JSR. This type of distribution leaves the flexible carbon black/binder less available to hold the particles together during the volume changes and associated stresses experienced during drying, which leads to cracks. We initial presented this hypothesis in a previous publication.[12] Overall, these results show that the nature of the binder strongly affects the distribution of the carbon/binder network within the coating, which in turn can affect the rate capability of the electrode.[29-31]

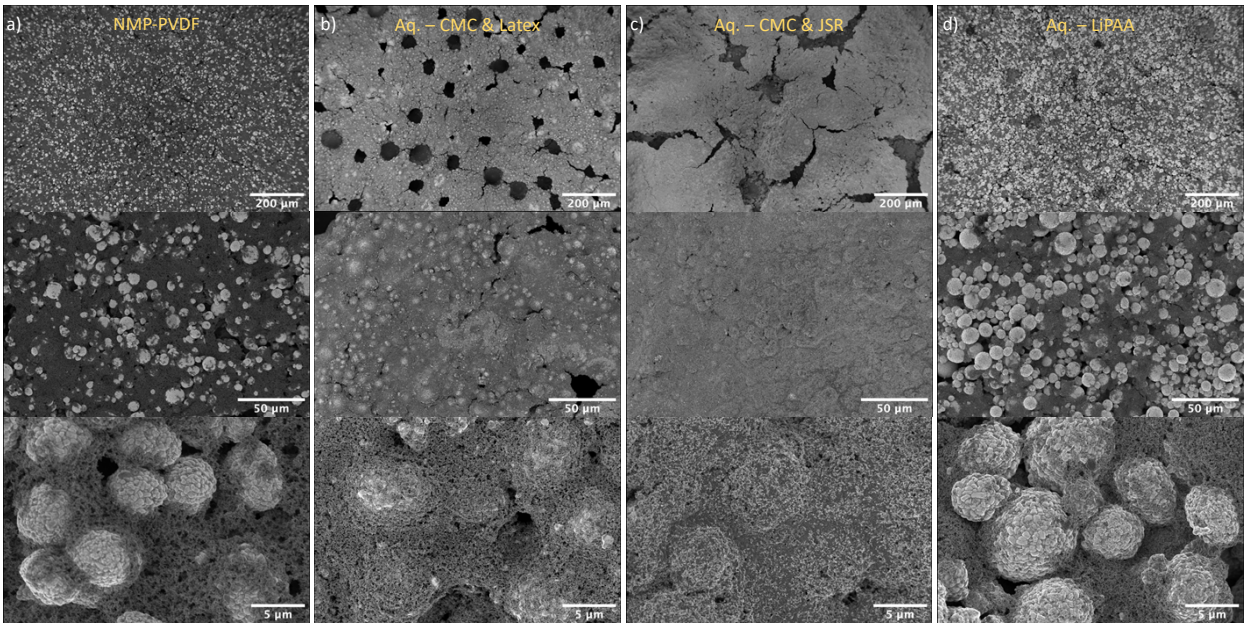


Figure 2 (a-d) SEM images of the surface of four types of cathode coatings at three different magnifications.

*Long-term cycling and rate capability analysis*

Figure 3a shows the long-term cycling performance of single-layer graphite//NMC 811 pouch cells made with all four cathodes (listed in Table 1) at a C/3 charge/discharge rate. All cells delivered similar initial discharge capacities of around 185-189 mAh $g^{-1}$. The discharge capacity of the baseline cells made with PVDF increased slightly at the beginning, which is a possible indication of incomplete electrolyte wetting, whereas the cells made with the three aqueous formulations started degrading from the beginning. Out of the three types of aqueous-based cells, the capacity fade for LiPAA-based cells was the most severe, while the CMC & JSR and CMC & Latex-based cells showed a slower capacity decay rate for the first ~600 cycles. The capacity fade decreased for the cells with LiPAA and CMC & JSR beyond ~600 cycles, whereas it increased in all three cells with CMC & Latex binder, making this binder the worst out of the four after 1000 cycles. Interestingly, the discharge capacity of the PVDF/NMP baseline cells was almost identical to the water-based CMC & JSR cells after 1000 cycles (~60% of their initial discharge capacity), even though they showed the slowest capacity fade during the first ~200 cycles. Therefore, the capacity retention can be correlated with binder choice as follows: PVDF > CMC & JSR ≈ CMC & Latex > LiPAA for the first ~600 cycles and CMC & JSR ≈ PVDF > LiPAA > CMC & Latex after 1000 cycles. These results reveal the significant influence of binder type on long-term cycling performance and demonstrate that aqueous-processed cells made with the right binder perform similarly to NMP-processed cells after 1000 cycles. We note that the difference in performance for the cells in this work (both NMP- and aqueous-processed) compared to our previous work[9] is likely due to the use of a different NMC811 starting material because the previous powder was no longer available.

The rate performance of a separate set of cells is shown in Figure 3b. Cells were charged at C/5 and discharged at different rates from C/10 to 5C. All cells showed similar discharge capacities of 195-197 mAh $g^{-1}$ at C/10. However, at higher rates up to 3C, the PVDF/NMP baseline cells demonstrated superior rate performance compared to all aqueous-based cells (159 mAh $g^{-1}$ for NMP-based vs. 136-144 mAh $g^{-1}$ for aqueous-based at 3C). Among the aqueous-processed cathodes, the ones made with CMC & Latex demonstrated the highest rate performance at C rates ≤ 2C, while the cells made with the other two binder systems were very similar. However, both the aqueous-processed and NMP-processed cells exhibited similar capacities at 5C.

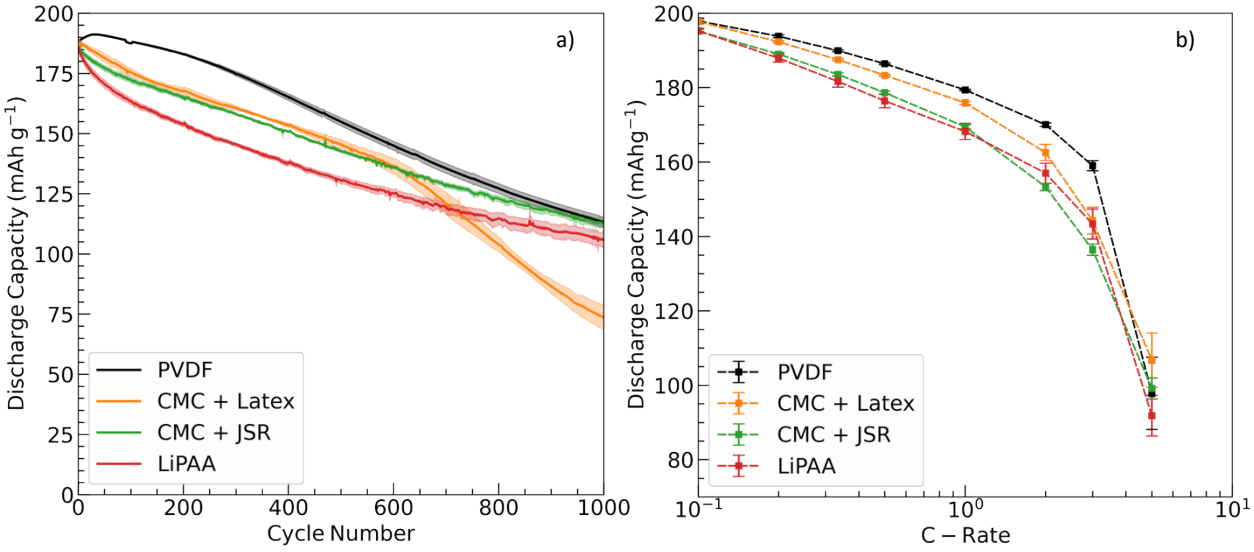


Figure 3. a) Long-term cycling performance (C/3 charge, C/3 discharge), and b) rate performance of single-layer graphite//NMC 811 pouch cells at 30 °C as a function of binder and solvent type used during cathode processing. Each data point is an average of three cells, and the error bars represent the standard deviation of these three cells.

We have observed similar rate performance behavior for the aqueous- and NMP-processed cells in our previous work investigating just one aqueous binder system.[9] We suggested that the difference in rate performance was due to either changes in the electrode microstructure or generation of insulating products at the interface from the corrosion of the aluminum substrate in the aqueous-processed cells. In this work, no clear correlation could be drawn between the microstructure of the coatings and their corresponding rate capability. For example, the baseline and aqueous-processed LiPAA binder coatings have similar microstructures with mostly bare NMC811 particles, but their rate performance was furthest apart (Figure 3b). Therefore, the primary contributing factor may be the presence of corrosion products at the cathode coating/aluminum interface. Since no pH modulating additives were used, the pH of all the water-based slurries was > 11, which is beyond the stability window of the aluminum foil substrate (Table 1). The microstructure also likely plays a role, but it is probably minor in comparison. More systematic studies that avoid the corrosion issue (for example, by employing a surface-protected aluminum foil) are needed to help answer that with certainty.

The direct current (DC) internal resistance of all pouch cells as a function of SOC was also measured during the long-term cycling via HPPC tests at an interval of every 200 cycles (Figure 4). The HPPC test is an alternative to AC impedance spectroscopy, intended to determine the dynamic power capability of a battery over its usable charge and voltage range. This is especially important for electric vehicle applications, where rapid charge/discharge during regenerative braking/acceleration can occur at any battery SOC.[32, 33] HPPC testing was performed by applying a series of fast (10 s long) discharge (2C) and charge (1.5C) steps to the cells at various SOCs.

Figure 4a-f shows the area specific impedance (ASI) plots as a function of SOC for all four types of cells at different cycle numbers. These are the same set of cells shown in Figure 3a. Figure 4g-h plots the ASI growth as a function of cycle number for two SOCs (~3.85 V and ~3.60 V). Although, the ASI includes contributions from all components of the cell, several studies on the aging of lithium-ion cells containing a layered cathode and graphite anode have shown that the cathode is the main contributor to the increase in cell impedance, while the contribution of the graphite anode is minimal.[34-36] HPPC tests of cells with a reference electrode have further shown that the resistance of the graphite anode is relatively constant throughout the voltage range of interest.[35, 37] Hence, the shape of the curves shown in Figure 4a-f can be reasonably attributed to cathode resistance. Before cycling, ASI differences between the cells made with NMP-processed and aqueous-processed cathodes are minimal. The steep increase in ASI at <3.5 V is typical for layered cathodes as they cannot intercalate/de-intercalate lithium ions at high rates at such low SOC.[38] The ASI trend observed at >3.6 V correlates well with that of the rate performance shown in Figure 3b. It is evident that the cell impedance increases with aging for all four cell types. Cells containing the LiPAA-binder cathodes showed the highest increase in resistance, while the baseline cells showed the lowest increase. Interestingly, cells containing the CMC & Latex-binder cathodes showed the second lowest resistance rise after 800 cycles, despite these cells showing a sudden drop in discharge capacity after 600 cycles. No corresponding sudden rise in cell resistance was observed. This could indicate that the accelerated capacity fade was not due to the increased resistance but rather probably due to cycling-induced detachment of NMC811 from the carbon black and binder network, resulting in electrically deactivated NMC811,[39] or lithium plating-induced active lithium loss. Overall, excluding the CMC & Latex-based cells, there is a clear similarity between the rate of ASI growth and the rate of discharge capacity fade (Figure 4g-h vs. Figure 4i).

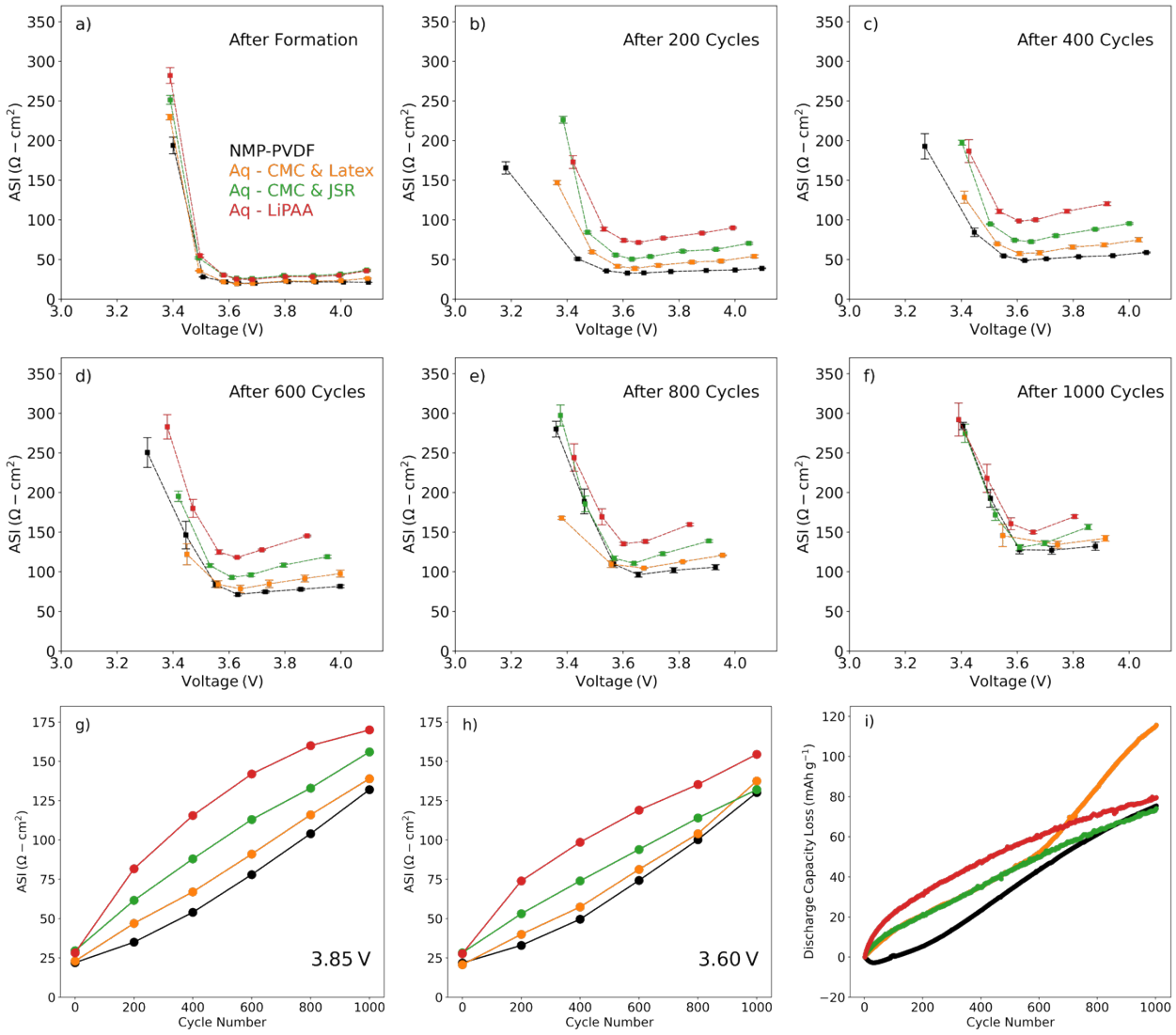


Figure 4. (a-f) Area specific impedance (ASI) as a function of voltage for single-layer graphite//NMC811 pouch cells, obtained via HPPC testing after formation, then after every 200 cycles during long-term cycling. (g-h) ASI values extracted from the HPPC plots at two different cell voltages (3.85 V and 3.60 V). (i) Cumulative loss of discharge capacity in mAh $g^{-1}$ compared to initial discharge capacity as a function of cycle number for all four types of cells.

To determine whether lithium plating is the main reason for capacity fade, long-term cycling performance of the best performing aqueous-processed cathode (with CMC & JSR binder) was also evaluated at an elevated temperature of 45 °C and compared with the PVDF/NMP baseline (Figure 5a). If lithium plating is the main reason for capacity fade, it will be mitigated at elevated temperature where the mass transport of lithium ions is improved. The PVDF/NMP baseline cells showed higher initial capacity and slower capacity fade over the first 200 cycles compared to the CMC & JSR-based cells (196 mAh $g^{-1}$ and 90 % vs. 184 mAh $g^{-1}$ and 80%). However, the baseline cells showed a higher capacity fade during later cycles compared to the aqueous-based cells. Between 200-400 cycles, baseline cells retained 81% of their original capacity whereas aqueous-

based cells retained 84%. This trend is similar to the capacity fade trend at room temperature, which shows that the capacity curves of the two cells will likely meet after another couple hundred cycles. However, comparing the capacities for the same cell type at two different temperatures, the aqueous-based cells retained 82% of the discharge capacity that they had retained at 30 °C by the 400$^{th}$ cycle compared to 87% for the baseline cells. In addition, the cell resistance of the baseline cells remained lower than that of the aqueous cells throughout cycling and increased at a lower rate (Figure 5b). The fact that the aqueous-based cells showed a greater degree of capacity fade at 45 °C compared to 30 °C suggests that mechanisms other than lithium plating are responsible for the faster capacity fade in aqueous-based cells, such as cycling-induced detachment of NMC 811 from the carbon black and binder network. An in-depth post-mortem study will be needed to elucidate with certainty the cause of the varying degrees of degradation with different binders.

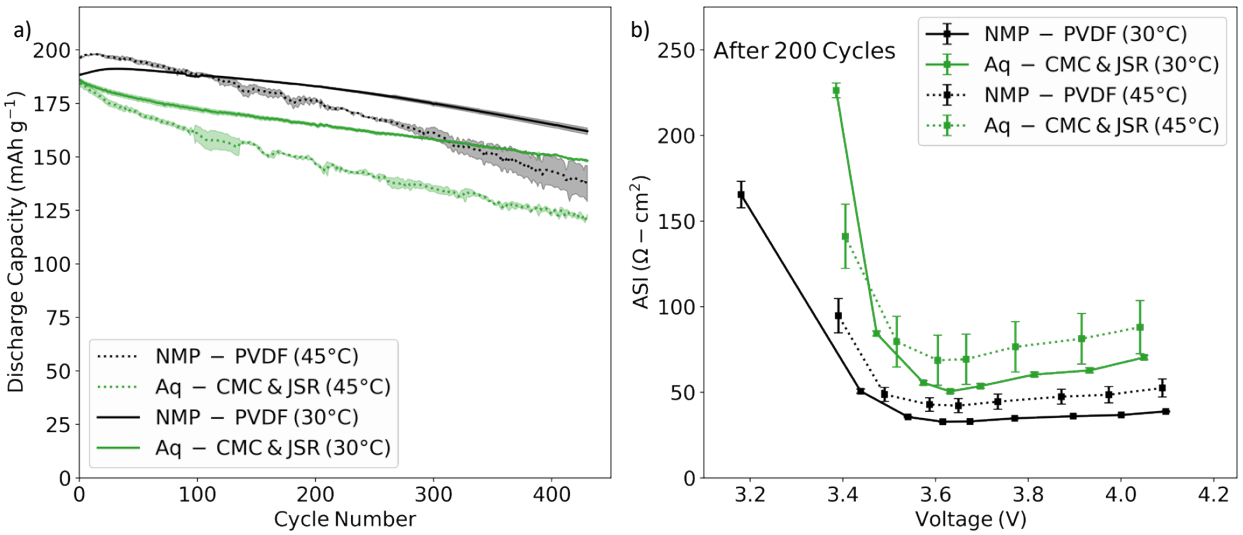


Figure 5. Long-term cycling performance (C/3 charge, C/3 discharge), and b) area specific impedance (ASI) of single-layer graphite//NMC811 pouch cells at 45 °C vs. 30 °C, made with either aqueous-processed CMC & JSR-binder cathodes or NMP-processed PVDF-binder cathodes.

## Conclusions

In conclusion, we demonstrated that the choice of water-based binder type for aqueous-processed NMC811 cathodes strongly impacts the long-term cycling performance of graphite//NMC 811 full cells. Despite a greater initial capacity fade, the aqueous-processed cells made with LiPAA or CMC & Latex binder showed similar capacity retention to the NMP-processed baseline cells made with PVDF after 1000 cycles (all about 60%). Conversely, the aqueous-processed cells made with CMC & Latex binder showed a dramatic capacity fade after ~600 cycles, demonstrating a final capacity retention of only 39 % after 1000 cycles. We found that the CMC & JSR binder was the best overall aqueous binder for long-term cycle life, with capacity retention correlating to binder choice as follows: PVDF > CMC & JSR ≈ CMC & Latex > LiPAA for the first ~600 cycles and CMC & JSR ≈ PVDF > LiPAA > CMC & Latex after 1000 cycles. The growth rate of cell

resistance obtained via HPPC testing correlated well with the capacity fade rate (except for the CMC & Latex-based cells). We note that the difference in the performance of the cells in this work (including the PVDF/NMP baseline) compared to our previous work is likely due to the use of a different NMC811 starting material, as the previous powder was no longer available.

While all of the cells demonstrated a similar capacity at C/10 and poor performance at 5C, the rate capability of the aqueous-processed cells was worse than the NMP-processed baseline cells at discharge rates between C/3 and 3C. However, the aqueous-processed cells made with the CMC & Latex binder performed better than those made with the other aqueous binders (PVDF > CMC & Latex > CMC & JSR ≈ LiPAA at discharge rates ≤ 3C). Interestingly, the different cathode microstructure and carbon black/binder distribution within the coatings did not seem to correlate with rate performance. This suggests that although the microstructure likely plays a minor role, the primary culprit of the rate performance difference is the formation of aluminum corrosion products at the coating/substrate interface due to the high pH of the aqueous slurries and/or poor adhesion to the current collector. The baseline NMP/PVDF slurry exhibited the best rheological behavior of all the samples, demonstrating the most elastic behavior in LVR tests as well as beneficial high- and low-shear viscosity behavior. The aqueous slurries had much lower storage moduli, implying a less robust binding network between particles in the slurry. However, they also displayed a lower viscosity, meaning that the solids loading could be further increased without sacrificing coating quality. This could lead to decreased manufacturing costs by reducing the amount of solvent used. Overall, these results show that if the correct binder system is chosen, aqueous-based cathode processing is promising as a more cost-effective, environmentally-friendly alternative to NMP-based processing, producing cells with a similar capacity retention after 1000 cycles.

**Acknowledgements**

This research at Oak Ridge National Laboratory, managed by UT Battelle, LLC, for the U.S. Department of Energy under contract DE-AC05-00OR22725, was sponsored by the Office of Energy Efficiency and Renewable Energy (EERE) Vehicle Technologies Office (VTO) (Deputy Director: David Howell) Applied Battery Research subprogram (Program Manager: Peter Faguy). SEM characterization was conducted at the Center for Nanophase Materials Sciences (CNMS), which is sponsored at Oak Ridge National Laboratory by the Division of Scientific User Facilities, U.S. Department of Energy, managed by UT-Battelle, LLC, for the U.S.

## References

1. Chen, H.; Ling, M.; Hencz, L.; Ling, H. Y.; Li, G.; Lin, Z.; Liu, G.; Zhang, S., Exploring chemical, mechanical, and electrical functionalities of binders for advanced energy-storage devices. *Chemical reviews* **2018,** *118* (18), 8936-8982.
2. Ma, Y.; Ma, J.; Cui, G., Small things make big deal: Powerful binders of lithium batteries and post-lithium batteries. *Energy Storage Materials* **2019,** *20*, 146-175.

3. Zou, F.; Manthiram, A., A Review of the Design of Advanced Binders for High‐Performance Batteries. *Advanced Energy Materials* **2020,** *10* (45), 2002508.
4. Wood III, D. L.; Li, J.; Daniel, C., Prospects for reducing the processing cost of lithium ion batteries. *Journal of Power Sources* **2015,** *275*, 234-242.
5. Wood, D. L.; Quass, J. D.; Li, J.; Ahmed, S.; Ventola, D.; Daniel, C., Technical and economic analysis of solvent-based lithium-ion electrode drying with water and NMP. *Drying technology* **2018,** *36* (2), 234-244.
6. Ahmed, S.; Nelson, P. A.; Gallagher, K. G.; Dees, D. W., Energy impact of cathode drying and solvent recovery during lithium-ion battery manufacturing. *Journal of Power Sources* **2016,** *322*, 169-178.
7. https://www.eia.gov/tools/faqs/faq.php?id=74&t=11.
8. Bresser, D.; Buchholz, D.; Moretti, A.; Varzi, A.; Passerini, S., Alternative binders for sustainable electrochemical energy storage–the transition to aqueous electrode processing and bio-derived polymers. *Energy & Environmental Science* **2018,** *11* (11), 3096-3127.
9. Wood, M.; Li, J.; Ruther, R. E.; Du, Z.; Self, E. C.; Meyer III, H. M.; Daniel, C.; Belharouak, I.; Wood III, D. L., Chemical stability and long-term cell performance of low-cobalt, Ni-Rich cathodes prepared by aqueous processing for high-energy Li-Ion batteries. *Energy Storage Materials* **2020,** *24*, 188-197.
10. Li, C.-C.; Lee, J.-T.; Tung, Y.-L.; Yang, C.-R., Effects of pH on the dispersion and cell performance of LiCoO 2 cathodes based on the aqueous process. *Journal of materials science* **2007,** *42* (14), 5773-5777.
11. Loeffler, N.; von Zamory, J.; Laszczynski, N.; Doberdo, I.; Kim, G.-T.; Passerini, S., Performance of LiNi1/3Mn1/3Co1/3O2/graphite batteries based on aqueous binder. *Journal of Power Sources* **2014,** *248*, 915-922.
12. Sahore, R.; Wood III, D. L.; Kukay, A.; Grady, K. M.; Li, J.; Belharouak, I., Towards understanding of cracking during drying of thick aqueous-processed LiNi0. 8Mn0. 1Co0. 1O2 cathodes. *ACS Sustainable Chemistry & Engineering* **2020,** *8* (8), 3162-3169.
13. Kimura, K.; Sakamoto, T.; Mukai, T.; Ikeuchi, Y.; Yamashita, N.; Onishi, K.; Asami, K.; Yanagida, M., Improvement of the cyclability and coulombic efficiency of Li-ion batteries using Li [Ni0. 8Co0. 15Al0. 05] O2 cathode containing an aqueous binder with pressurized CO2 gas treatment. *Journal of The Electrochemical Society* **2018,** *165* (2), A16.
14. Bauer, W.; Çetinel, F. A.; Müller, M.; Kaufmann, U., Effects of pH control by acid addition at the aqueous processing of cathodes for lithium ion batteries. *Electrochimica Acta* **2019,** *317*, 112-119.
15. Doberdò, I.; Löffler, N.; Laszczynski, N.; Cericola, D.; Penazzi, N.; Bodoardo, S.; Kim, G.-T.; Passerini, S., Enabling aqueous binders for lithium battery cathodes–Carbon coating of aluminum current collector. *Journal of power sources* **2014,** *248*, 1000-1006.
16. Kukay, A.; Sahore, R.; Parejiya, A.; Hawley, W. B.; Li, J.; Wood III, D. L., Aqueous Ni-rich-cathode dispersions processed with phosphoric acid for lithium-ion batteries with ultra-thick electrodes. *Journal of Colloid and Interface Science* **2021,** *581*, 635-643.
17. Loeffler, N.; Kim, G. T.; Mueller, F.; Diemant, T.; Kim, J. K.; Behm, R. J.; Passerini, S., In situ coating of Li [Ni0. 33Mn0. 33Co0. 33] O2 particles to enable aqueous electrode processing. *ChemSusChem* **2016,** *9* (10), 1112-1117.
18. Memm, M.; Hoffmann, A.; Wohlfahrt-Mehrens, M., Water-based LiNi1/3Mn1/3Co1/3O2-cathodes with good electrochemical performance by use of additives. *Electrochimica Acta* **2018,** *260*, 664-673.
19. Hawley, W. B.; Meyer III, H. M.; Li, J., Enabling aqueous processing for LiNi0. 80Co0. 15Al0. 05O2 (NCA)-based lithium-ion battery cathodes using polyacrylic acid. *Electrochimica Acta* **2021,** *380*, 138203.

20. Li, J.; Rulison, C.; Kiggans, J.; Daniel, C.; Wood III, D. L., Superior performance of LiFePO4 aqueous dispersions via corona treatment and surface energy optimization. *Journal of The Electrochemical Society* **2012,** *159* (8), A1152.
21. An, S. J.; Li, J.; Mohanty, D.; Daniel, C.; Polzin, B. J.; Croy, J. R.; Trask, S. E.; Wood, D. L., Correlation of electrolyte volume and electrochemical performance in lithium-ion pouch cells with graphite anodes and NMC532 cathodes. *Journal of The Electrochemical Society* **2017,** *164* (6), A1195.
22. Bauer, W.; Nötzel, D., Rheological properties and stability of NMP based cathode slurries for lithium ion batteries. *Ceramics International* **2014,** *40* (3), 4591-4598.
23. Bitsch, B.; Dittmann, J.; Schmitt, M.; Scharfer, P.; Schabel, W.; Willenbacher, N., A novel slurry concept for the fabrication of lithium-ion battery electrodes with beneficial properties. *Journal of Power Sources* **2014,** *265*, 81-90.
24. Hawley, W. B.; Li, J., Beneficial rheological properties of lithium-ion battery cathode slurries from elevated mixing and coating temperatures. *Journal of Energy Storage* **2019,** *26*, 100994.
25. Mewis, J.; Wagner, N. J., *Colloidal suspension rheology*. Cambridge university press: 2012.
26. Björn, A.; de La Monja, P. S.; Karlsson, A.; Ejlertsson, J.; Svensson, B. H., Rheological characterization. *Biogas* **2012,** *1*, 63-76.
27. Bitsch, B.; Dittmann, J.; Schmitt, M.; Scharfer, P.; Schabel, W.; Willenbacher, N., A novel slurry concept for the fabrication of lithium-ion battery electrodes with beneficial properties. *Journal of Power Sources* **2014,** *265*, 81--90.
28. Ibing, L.; Gallasch, T.; Schneider, P.; Niehoff, P.; Hintennach, A.; Winter, M.; Schappacher, F. M., Towards water based ultra-thick Li ion battery electrodes–a binder approach. *Journal of Power Sources* **2019,** *423*, 183-191.
29. Zheng, H.; Yang, R.; Liu, G.; Song, X.; Battaglia, V. S., Cooperation between active material, polymeric binder and conductive carbon additive in lithium ion battery cathode. *The Journal of Physical Chemistry C* **2012,** *116* (7), 4875-4882.
30. Srivastava, I.; Bolintineanu, D. S.; Lechman, J. B.; Roberts, S. A., Controlling Binder Adhesion to Impact Electrode Mesostructures and Transport. *ACS applied materials & interfaces* **2020,** *12* (31), 34919-34930.
31. Chouchane, M.; Rucci, A.; Lombardo, T.; Ngandjong, A. C.; Franco, A. A., Lithium ion battery electrodes predicted from manufacturing simulations: Assessing the impact of the carbon-binder spatial location on the electrochemical performance. *Journal of Power Sources* **2019,** *444*, 227285.
32. Abraham, D.; Dees, D.; Christophersen, J.; Ho, C.; Jansen, A., Performance of high‐power lithium‐ion cells under pulse discharge and charge conditions. *International Journal of Energy Research* **2010,** *34* (2), 190-203.
33. Christophersen, J. P. *Battery Test Manual For Electric Vehicles, Revision 3*; Idaho National Lab.(INL), Idaho Falls, ID (United States): 2015.
34. Gilbert, J. A.; Bareño, J.; Spila, T.; Trask, S. E.; Miller, D. J.; Polzin, B. J.; Jansen, A. N.; Abraham, D. P., Cycling behavior of NCM523/graphite lithium-ion cells in the 3–4.4 V range: diagnostic studies of full cells and harvested electrodes. *Journal of The Electrochemical Society* **2016,** *164* (1), A6054.
35. Li, Y.; Bettge, M.; Polzin, B.; Zhu, Y.; Balasubramanian, M.; Abraham, D. P., Understanding long-term cycling performance of Li1. 2Ni0. 15Mn0. 55Co0. 1O2–graphite lithium-ion cells. *Journal of The Electrochemical Society* **2013,** *160* (5), A3006.
36. Chen, C.; Liu, J.; Amine, K., Symmetric cell approach and impedance spectroscopy of high power lithium-ion batteries. *Journal of Power Sources* **2001,** *96* (2), 321-328.
37. An, S. J.; Li, J.; Daniel, C.; Kalnaus, S.; Wood III, D. L., Design and demonstration of three-electrode pouch cells for lithium-ion batteries. *Journal of the Electrochemical Society* **2017,** *164* (7), A1755.

38. Shaju, K.; Rao, G. S.; Chowdari, B., Influence of Li-Ion Kinetics in the Cathodic Performance of Layered Li (Ni1/3Co1/3Mn1/3) O 2. *Journal of the Electrochemical Society* **2004,** *151* (9), A1324.
39. Liu, H.; Foster, J. M.; Gully, A.; Krachkovskiy, S.; Jiang, M.; Wu, Y.; Yang, X.; Protas, B.; Goward, G. R.; Botton, G. A., Three-dimensional investigation of cycling-induced microstructural changes in lithium-ion battery cathodes using focused ion beam/scanning electron microscopy. *Journal of Power Sources* **2016,** *306*, 300-308.